AIAA JOURNAL
Vol. 60, No. 6, June 2022

Active Control of Multiple Neural Networks for Oscillating Combustion

Long Zhang,* Xingyu Su,† Hua Zhou,‡ Xiangyang Wang,§ and Zhuyin Ren¶
Tsinghua University, 100084 Beijing, People's Republic of China

https://doi.org/10.2514/1.J061370

A multiple neural network controller is proposed and demonstrated to suppress the pressure oscillation of the Rijke tube acoustic network. This controller consists of three modules including two separate neural networks, i.e., the neural network of controlled object that is pretrained before control and the neural network of controller that is trained in real time during the control process. This controller can identify the characteristics of oscillating combustion, achieve adaptive output, and extend the applicability and expansibility. Results show that multiple neural network controller can suppress the pressure oscillation in different oscillating stages using fuel valve or loudspeaker as actuators. When the exact mathematical model of the controlled object is difficult to obtain, it is effective to take a zero-dimensional simplified model with similar oscillating characteristics for prototype controller, and then actively control the real controlled object through parameter migration. It is further demonstrated that this controller is insensitive to noise. In addition, delay correction is achieved by adding sensor and actuator delay modules to the original controller to offset the effects of system delay.

I. Introduction

OSCILLATING combustion is a phenomenon of combustion instability in rocket engine [1–5], aero-engine afterburner [6–10], lean premixed heavy duty gas turbine [11–14], and industrial furnaces [15–19], which has adverse effects on combustion system and attracts wide attentions. Oscillating combustion is a mutually excited cyclic oscillation process when the unsteady heat release frequency in a combustion chamber is close to the characteristic frequency of the geometric structure [20]. In the intrinsic acoustic mode of the combustion chamber, the inherent disturbance of the system is self-excited through the interaction with the combustion process, forming large-amplitude pressure, velocity, and heat release fluctuations [21,22]. The amplitude of pressure fluctuations increases linearly with time at the initial stage of oscillating combustion. Affected by nonlinear mechanisms such as the increase of sound energy dissipation or the phase change between unsteady heat release fluctuation and pressure fluctuation, this pressure amplitude tends to be saturated and finally reaches the limit cycle state [5,6,21–23].

Currently, two types of approaches are widely adopted to investigate oscillating combustion. One is 3D compressible computational fluid dynamics simulation [13,24–27] resolving the unsteady heat release and acoustic oscillation simultaneously, which is relatively time-consuming, and sensitive to numerical schemes, turbulence, and combustion models and boundary conditions. The other is a low-order acoustic network model, which simplifies the combustor structure into a series of simple geometric units, decouples the acoustic process from the combustion process, and consequently requires small demand for computing resources [8,28–32]. For example, Gonzalez-Flesca et al. [29] described a reduced-order numerical framework to simulate combustion instabilities in liquid rocket engines, which relied on the projection of the pressure fluctuations on the eigenmodes of the system. After projection on the eigenmodes, the wave equation takes the form of a series of second-order harmonic equations with source terms that drive combustion instabilities and damping terms that attenuate them. The predictions from this reduced-order approach were validated against with the experimental data. Mahmoudi et al. [30] presented a low-order model to study the propagation and interaction of acoustic and entropic perturbations through a convergent–divergent nozzle. The calculations considered choked, unchoked, as well as compact and noncompact nozzles. Results showed that the entropy noise was the main source of noise downstream of the choked nozzle and the vorticity noise had a negligible contribution. This low-order model was in excellent agreement with the experimental results of the entropy wave generator and hot acoustic test rig.

In the design process of oscillating combustion controller, it is necessary to construct a simplified model of the controlled object, so as to effectively capture the oscillating characteristics of the controlled object and quickly respond to the controller output [33–36]. Using low-dimensional acoustic network as this simplified model is an effective solution when the exact mathematical model of the controlled object is difficult to obtain. Considerable researches have been reported on developing various oscillating combustion controllers based on a low-dimensional acoustic network model, due to its rapid yet reliable capture of the oscillating characteristics [37–39].

Both passive control and active control can be adopted to suppress the oscillating combustion. For passive control, oscillating combustion is inhibited at specific frequencies by adjusting combustion organization or using acoustic resonators [40–42]. For active control, the sensor measurements are obtained for the calculation of active control algorithm, and the controller output is dynamically adjusted to suppress the oscillating process [33–36]. Due to the flexibility and adaptability of active control, various types of active controllers have been developed in recent years [39], including phase shift controller [39,43], linear optimal controller [43,44], time-delay controller [45], and adaptive controller [46,47]. Chae and Lee [33] conducted a series of combustion tests to actively control and suppress the initiation of low-frequency instability by using fuel inserts. Results showed that fuel insert could delay the low-frequency instability, and the number and locations of the fuel inserts played important roles in determining the level of suppression as well as the phase difference between the pressure and heat release oscillations. Properly locating two fuel inserts simultaneously in the axial direction could suppress the oscillating combustion completely. John et al. [36] demonstrated active combustion instability suppression using the adaptive sliding phasor average control method in a combustion test cell operating at engine-relevant pressure, temperature, and flow conditions. With a

Received 14 October 2021; revision received 26 December 2021; accepted for publication 7 February 2022; published online 11 March 2022.

*Ph.D. Student, School of Aerospace Engineering; long-zha19@mails.tsinghua.edu.cn.
†Ph.D. Student, Department of Energy and Power Engineering; su-xy19@mails.tsinghua.edu.cn.
‡Assistant Professor, Institute for Aero Engine; zhouhua@tsinghua.edu.cn.
§Assistant Professor, Institute for Aero Engine; wangxy668@tsinghua.edu.cn.
¶Professor, Institute for Aero Engine; zhuyinren@tsinghua.edu.cn. Associate Fellow AIAA.

high-frequency fuel valve for the inflowing fuel perturbation and a dynamic pressure sensor in the combustor for controller feedback, successful instability suppression was achieved when combustor operation transitions from a stable low-power condition to a normally unstable high-power condition.

In our previous study [47], a neural network Proportional Integral Derivative (PID) controller is attempted to achieve the active control of oscillating combustion in a Rijke tube. The controller consists of the conventional PID component and a neural network component, where the PID control parameters are adjusted in real time by the neural network based on the system working conditions. In this controller configuration, the PID controller directly controls the controlled object. Although this controller can effectively suppress the oscillating reference pressure of a Rijke tube model system under certain circumstances, it has deficiencies in the adaptability of the controlled object. It needs an accurate mathematical model of the controlled object to build the control algorithm, and needs time-consuming empirical PID parameter tuning. Moreover, this controller does not consider the ubiquitous effects of system delay. In this study, a multiple neural network controller is proposed to address these challenges. It is demonstrated to suppress the pressure oscillation of the Rijke tube model system with its dynamics being governed by an analytical acoustic network model. Taking the Rijke tube acoustic network model as the controlled object, this active controller identifies and learns the oscillating combustion model through the neural network of controlled object, which enhances the adaptability of this controller to the controlled object due to the highly nonlinear generalization of neural network. Another neural network of controller is adopted to achieve the adaptive output. The effects of system delay on the performance of controller are studied in detail. Parameter migration method is used to initialize the controller parameters of the Rijke tube acoustic network model, which avoids the empirical tuning of PID parameters.

The remainder of this paper is organized as follows. In Sec. II, the Rijke tube acoustic network model is introduced, followed by the description of the multiple neural network controller. In Sec. III, the performance of this controller and the effects of parameter migration, noise, and system delay are analyzed in detail. Conclusions are drawn in Sec. IV.

II. Methodology

A. Rijke Tube Acoustic Network Model

Rijke tube provides the simplest means of obtaining combustion instabilities on a laboratory scale, and it is widely adopted as controlled object in the research of oscillating combustion control [37,38,47–49]. For example, Morgans and Dowling [37] designed a model-based active controller for a laboratory-scale Rijke tube combustion system as shown in Fig. 1a. A propane-fuelled Bunsen burner provided a flat laminar flame, which was stabilized on a grid. A microphone and loudspeaker were adopted as sensor and actuator, respectively. The unstable open-loop transfer function was measured experimentally. With the assumptions of compact combustion zone, ignoring the dissipation of acoustic waves, neglecting the entropy wave, and considering only longitudinal wave, a low-order acoustic network model was formulated to model the pressure oscillation in this Rijke tube system. A robust model-based controller is then designed and implemented based on the simulation results of the acoustic network model.

In this study, as shown in Fig. 1b, a cylindrical Rijke tube model system with a constant cross section and both ends open is employed to demonstrate the active control oscillating combustion with multiple neural networks. The inlet and outlet of the Rijke tube locate at $x = -x_1$ and $x = x_2$. An ethylene premixed flame is used as the heat source of the system. Following the same assumptions as in [37], the acoustic wave can be described by the superposition of forward and backward propagating plane waves considering that only the longitudinal waves are taken into account. Two kinds of independent control actuators are adopted: one is the loudspeaker locating at the tube inlet, and the other is the fuel valve that affects the characteristics of the system oscillation by changing the heat release characteristics at the flame location. A microphone sensor is adopted at $x = x_r$. Denote the upstream and downstream regions of the premixed flame by subscripts 1 and 2, the mean flow variables with an overbar, and small perturbations with a prime. The corresponding analytical acoustic network model as in [37,38,47–49] is given by

$$p_1(x,t) = \bar{p}_1 + p_1'(x,t) = \bar{p}_1 + A_1^+(t-\tau_1^+) + A_1^-(t+\tau_1^-) \quad (1)$$

$$u_1(x,t) = \bar{u}_1 + u_1'(x,t) = \bar{u}_1 + \frac{1}{\bar{\rho}_1\bar{c}_1}[A_1^+(t-\tau_1^+) - A_1^-(t+\tau_1^-)] \quad (2)$$

$$p_2(x,t) = \bar{p}_2 + p_2'(x,t) = \bar{p}_2 + A_2^+(t-\tau_2^+) + A_2^-(t+\tau_2^-) \quad (3)$$

$$u_2(x,t) = \bar{u}_2 + u_2'(x,t) = \bar{u}_2 + \frac{1}{\bar{\rho}_2\bar{c}_2}[A_2^+(t-\tau_2^+) - A_2^-(t+\tau_2^-)] \quad (4)$$

$$\tau_1^+ = \frac{x}{\bar{c}_1 + \bar{u}_1} \quad (5)$$

$$\tau_1^- = \frac{x}{\bar{c}_1 - \bar{u}_1} \quad (6)$$

$$\tau_2^+ = \frac{x}{\bar{c}_2 + \bar{u}_2} \quad (7)$$

$$\tau_2^- = \frac{x}{\bar{c}_2 - \bar{u}_2} \quad (8)$$

where u and c represent the velocity and speed of sound, τ denotes the time delay, A^+ and A^- represent the amplitudes of the backward and forward propagating plane waves. Considering the conservation of mass, momentum, and energy together with the equation of state for perfect gas, the governing equation in the Laplace domain for this Rijke tube model system is given by

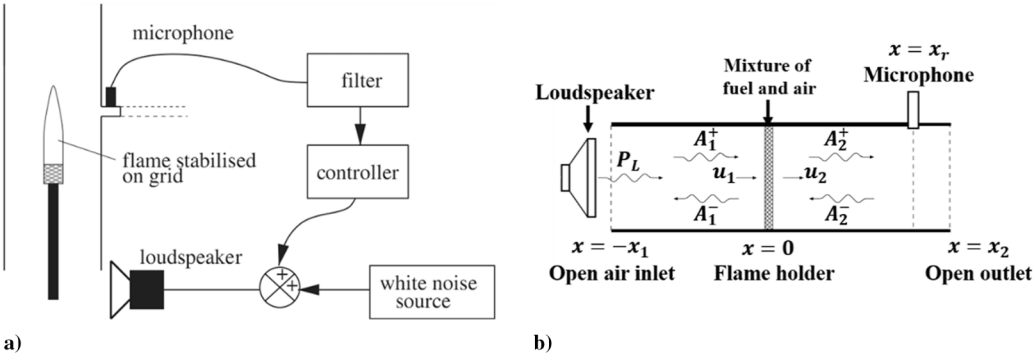

Fig. 1 Schematic diagram of a) the Rijke tube system and b) the corresponding model system for acoustic network model.

$$\begin{bmatrix} X_{11} & X_{12} \\ X_{21} & X_{22} \end{bmatrix} \begin{bmatrix} A_1^-(s) \\ A_2^+(s) \end{bmatrix} + \begin{bmatrix} Y_{11} & Y_{12} \\ Y_{21} & Y_{22} \end{bmatrix} \begin{bmatrix} R_1(s)A_1^-(s)e^{-\tau_1 s} \\ R_2(s)A_2^+(s)e^{-\tau_2 s} \end{bmatrix} = \begin{bmatrix} 0 \\ -1 \end{bmatrix} \frac{\dot{q}'(s)}{\bar{c}_1} \tag{9}$$

where R_1 and R_2 represent the pressure reflection coefficients at the inlet and outlet. The components of matrices $\boldsymbol{X}$ and $\boldsymbol{Y}$ are given by

$$\boldsymbol{X} = \begin{pmatrix} -1 + \bar{M}_1\left(2 - \frac{\bar{u}_2}{\bar{u}_1}\right) - \bar{M}_1^2\left(1 - \frac{\bar{u}_2}{\bar{u}_1}\right) & 1 + \bar{M}_1 \frac{\bar{\rho}_1 \bar{c}_1}{\bar{\rho}_2 \bar{c}_2} \\ \frac{1-\gamma\bar{M}_1}{\gamma-1} + \bar{M}_1^2 - \frac{\bar{M}_1^2}{2}(1-\bar{M}_1)\left(\frac{\bar{u}_2^2}{\bar{u}_1^2} - 1\right) & \frac{\bar{c}_2}{\bar{c}_1}\frac{1+\gamma\bar{M}_2}{\gamma-1} + \bar{M}_1\bar{M}_2\frac{\bar{\rho}_1}{\bar{\rho}_2} \end{pmatrix} \tag{10}$$

$$\boldsymbol{Y} = \begin{pmatrix} \frac{1-\bar{M}_1}{1+\bar{M}_1}\left(1 - \bar{M}_1\left(2 - \frac{\bar{u}_2}{\bar{u}_1}\right) + \bar{M}_1^2\left(1 - \frac{\bar{u}_2}{\bar{u}_1}\right)\right) & 1 - \bar{M}_1\frac{\bar{\rho}_1\bar{c}_1}{\bar{\rho}_2\bar{c}_2} \\ \frac{1-\bar{M}_1}{1+\bar{M}_1}\left(\frac{1+\gamma\bar{M}_1}{\gamma-1} + \bar{M}_1^2 - \frac{\bar{M}_1^2}{2}(1+\bar{M}_1)\left(\frac{\bar{u}_2^2}{\bar{u}_1^2} - 1\right)\right) & -\frac{\bar{c}_2}{\bar{c}_1}\frac{1-\gamma\bar{M}_2}{\gamma-1} - \bar{M}_1\bar{M}_2\frac{\bar{\rho}_1}{\bar{\rho}_2} \end{pmatrix} \tag{11}$$

where $\bar{M}$ represents the Mach number. The heat release perturbation $\dot{q}'$ is described by the following flame model [50,51]:

$$\frac{\dot{q}'(s)}{\bar{\dot{q}}} = \mathcal{T}(s)\left(\frac{u'(s)}{\bar{u}} - \frac{\phi'(s)}{\bar{\phi}}\right) \tag{12}$$

$$\mathcal{T}(s) = \frac{\omega_c}{s + \omega_c} n_f e^{-\tau_f s} \tag{13}$$

where $\mathcal{T}$ represents the flame function, ϕ denotes the equivalence ratio, n_f, ω_c, and τ_f represent the gain, cutoff angular frequency, and time delay, respectively. In this study, ω_c is 200π, τ_f is 0.001 s, and n_f is determined as in [52] by

$$n_f = \int_0^{\hat{u}_1/\bar{u}_1} \frac{1}{1 + (\alpha + 0.85)^{30}}\, \mathrm{d}\alpha \tag{14}$$

where $\hat{u}$ represents the velocity amplitude.

The governing equations are slightly different when the fuel valve or loudspeaker is used as actuators. When using fuel valve, the instantaneous flow rate is changed, and equivalence ratio fluctuations are generated, which affects the last term of Eq. (12), and then affects the $\dot{q}'$ term in Eq. (9). The governing equations solved are Eqs. (1–14). When using loudspeaker, the pressure generated by the loudspeaker acts directly on the longitudinally propagating oscillating combustion pressure field. Equations (1), (2), and (9) become

$$p_1(x,t) = \bar{p}_1 + A_1^+(t - \tau_1^+) + A_1^-(t + \tau_1^-) + P_L(t - \tau_1^+) \tag{15}$$

$$u_1(x,t) = \bar{u}_1 + \frac{1}{\bar{\rho}_1\bar{c}_1}[A_1^+(t - \tau_k^+) - A_1^-(t + \tau_k^-) + P_L(t - \tau_1^+)] \tag{16}$$

$$\begin{bmatrix} X_{11} & X_{12} \\ X_{21} & X_{22} \end{bmatrix} \begin{bmatrix} A_1^-(s) \\ A_2^+(s) \end{bmatrix} + \begin{bmatrix} Y_{11} & Y_{12} \\ Y_{21} & Y_{22} \end{bmatrix} \begin{bmatrix} R_1(s)A_1^-(s)e^{-\tau_1 s} + P_L(s)e^{-\tau_L s} \\ R_2(s)A_2^+(s)e^{-\tau_2 s} \end{bmatrix} = \begin{bmatrix} 0 \\ -1 \end{bmatrix} \frac{\dot{q}'(s)}{\bar{c}_1} \tag{17}$$

where P_L represents the loudspeaker sound signal, and τ_L is the loudspeaker time delay. Hence the governing equations solved are Eqs. (3–8) and (10–17).

Table 1 Geometric parameters and thermodynamic conditions of the Rijke tube model system

Item	Unit	Value
x_1	M	0.8
x_2	M	1.0
x_r	M	0.5
$\bar{P}_1$	Pa	101,325
$\bar{T}_1$	K	300
$\bar{M}_1$	——	0.11
Gas	——	Ethylene
Eff	——	0.8
ϕ	——	0.7
R_1	——	−1
R_2	——	−1

The geometric parameters and thermodynamic conditions of the Rijke tube model system are listed in Table 1, where "Eff" represents the combustion efficiency.

Figure 2 shows the evolution of pressure oscillation normalized by atmospheric pressure, growth rate, and frequency of the Rijke tube model. The growth rate is expressed in terms of the change rate in the natural logarithm of pressure oscillation amplitude. As shown, with the nonlinear flame model, the normalized pressure oscillation can be divided into three stages: linear growth stage, transition stage, and saturation stage. In the linear growth stage, the growth rate of the pressure oscillation remains unchanged at 5.86 s^{-1}. In the transition stage, the growth rate gradually decreases from 5.86 s^{-1} to 0, and the pressure oscillation is saturated. In the saturation stage, the pressure oscillation amplitude is saturated at 2956 Pa, and the system oscillation frequency remains 135.5 Hz.

B. Multiple Neural Network Controller

The specific structure of the multiple neural network controller adopted is shown in Fig. 3, where u_c denotes the controller output, $\boldsymbol{p}_0$ represents the oscillating pressures at several continuous historical

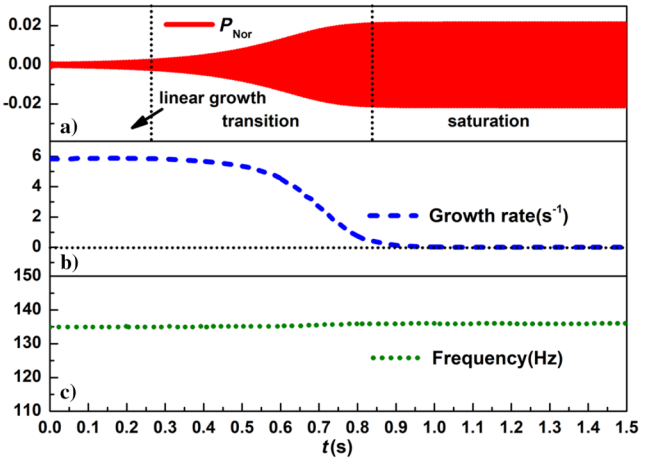

Fig. 2 Oscillation evolution of the Rijke tube model. a) Normalized pressure; b) growth rate; c) frequency.

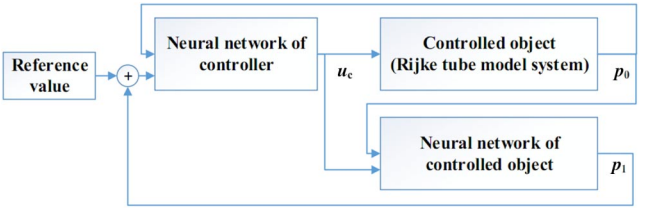

Fig. 3 Structure of the multiple neural network controller.

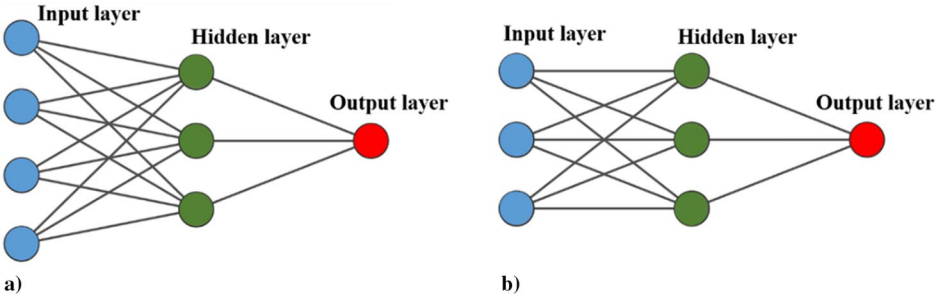

Fig. 4 Neural network structures of a) controlled object and b) controller.

times, and p_1 represents the predicted pressure at the next moment. This controller takes the Rijke tube model system of Fig. 1b as the controlled object, and consists of three modules including two separate neural networks, one for controlled object and the other for the controller. The neural network of controlled object is used to predict the future data p_1 of the controlled object through the historical data $\boldsymbol{p}_0$ of the controlled object and the controller output u_c. It is pretrained using a flat-band signal taken from pseudorandom number series for the training set and a step signal for the validation set. The root-mean-squared errors between the outputs of this neural network and the Rijke tube acoustic network model are used as the loss function. The neural network of controller is trained in real time through historical data $\boldsymbol{p}_0$, future data p_1 of the controlled object, and system reference values. The controller output u_c at the next moment is outputted for the calculation of the Rijke tube acoustic network model and neural network of the controlled object.

The neural network structures of controlled object and controller are shown in Fig. 4. The neural network of controlled object adopts a three-layer backpropagation neural network structure consisting of four input neurons, three hidden neurons, and one output neuron. The four input neurons correspond to three historical data $\boldsymbol{p}_0$ of controlled object and the controller output u_c at the current moment. The one output neuron corresponds to the future data p_1 at the next moment. The inputs and outputs of hidden and output layers are shown as follows:

$$\text{net}_h(t) = \boldsymbol{W_i K} = \sum_{m=1}^{4} w_{im} k_m \tag{18}$$

$$O_h(t) = f(\text{net}_h(t)) \tag{19}$$

$$f(x) = \frac{e^x - e^{-x}}{e^x + e^{-x}} \tag{20}$$

$$\text{net}_o(t) = \sum_{n=1}^{3} w_{hn} O_{hn} \tag{21}$$

$$O_o(t) = f(\text{net}_o(t)) \tag{22}$$

$$L = (p_1 - \theta)^2 \tag{23}$$

where $\boldsymbol{K}$ represents the input neurons, w_i and w_h are the weights of input and hidden layers, net_h and net_o are the total inputs of hidden and output neurons, O_h and O_o are the outputs of hidden and output neurons, f is the hyperbolic tangent activation function, and L is the loss function. The neural network of controller adopts a three-layer neural network structure, including three input neurons, three hidden neurons, and one output neuron. The three input neurons correspond to three historical data $\boldsymbol{p}_0$ of controlled object, and the one output neuron corresponds to the controller output u_c at the next moment. The loss function is the mean-squared error between the reference value θ and the predicted future data p_1 from the neural network of the controlled object. For the Rijke tube model system considered in this study, the above neural network structure and the number of neurons can meet the requirements of controller design. For more complex controlled objects, the structure and the number of neurons for these two neural networks may need to be adjusted. In addition, the clustering prediction method [16] could be employed to improve the prediction accuracy of neural network especially for controlled objects with complex dynamic phenomena or long-term prediction requirements.

The workflow of this multiple neural network controller is as follows:

1) Use the flat-band output signal taken from pseudorandom number series and the step output signal to construct training and validation sets for the neural network of controlled object.

2) Pretrain the neural network of controlled object to obtain the approximation model of the Rijke tube acoustic network.

3) Build the multiple neural network controller and set the reference value.

4) Optimize the neural network of controller in real time to suppress the oscillating combustion of the controlled object.

III. Results and Discussion

A. Performance of Multiple Neural Networks Controller

The training and validation sets for the neural network of controlled object using fuel valve as actuator are shown in Fig. 5, with the number of data in the training and validation sets being the same of 150,000. Figures 5a and 5c are the controller outputs of the training and validation sets, and Figs. 5b and 5d are the normalized pressure oscillations, respectively. With the effects of the flat-band output signal taken from pseudorandom number series, the pressure oscillated randomly, and the pressure oscillation amplitude was within ± 0.03. With the effects of the step output signal, the pressure oscillated violently in the initial stage with an oscillation amplitude of ± 0.22, and then gradually attenuated to a periodic oscillation of ± 0.03. The significant differences between the training and validation sets were beneficial for the neural network of controlled object to learn the characteristics of the nonlinear Rijke tube acoustic network.

Figure 6 shows the training results of the neural network of controlled object. The evolutions of training results, validation results, and loss function are shown in Figs. 6a–6c, respectively. With the increase of the number of training cycles, this neural network could fit the variation trend of system pressure with high precision under the effects of the flat-band and step output signals. The root-mean-squared errors decreased rapidly and finally remained constant, which indicated that the neural network training ended, and the weights reached the optimal results. These weights of the neural network of controlled object remained unchanged in the subsequent multiple neural network control process.

Figures 7 and 8 show the active control results of the multiple neural network controller using fuel valve as actuator. The starting times of control were 0.5 and 1.0 s corresponding to the transition and saturation stages of oscillating pressure as shown in Fig. 2, so as to investigate the ability of this controller to suppress the oscillating combustion at different stages. The normalized pressure, controller output, and the weights evolution of the hidden layer of the neural network of controller are shown in Figs. 7a–7d, respectively. Those of the output layer are shown in Figs. 8a–8d. It can be seen that the evolution of system pressure before control was consistent with that

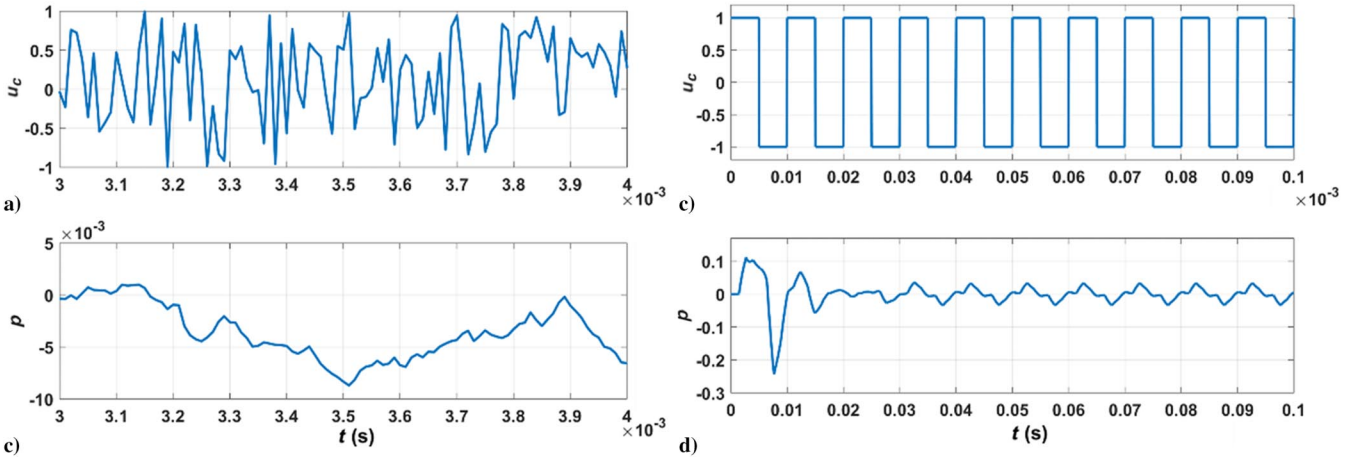

Fig. 5 Training and validation sets of the neural network of controlled object (fuel valve actuator). a) Controller output for training; b) normalized pressure for training; c) controller output for validation; d) normalized pressure for validation.

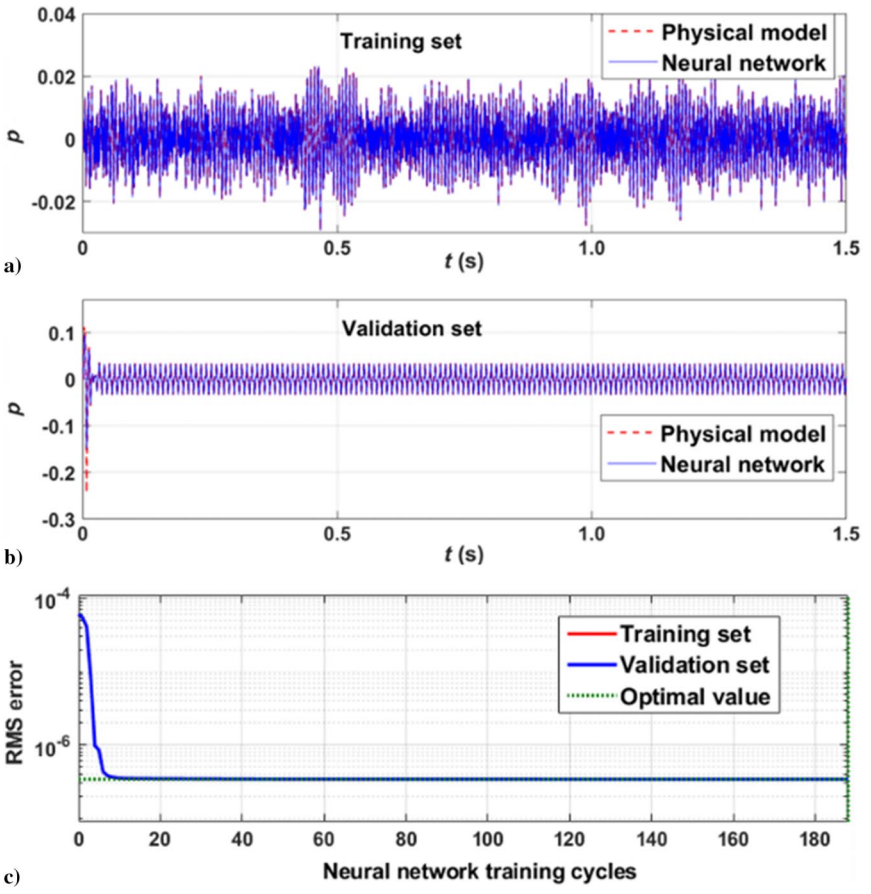

Fig. 6 Training results of the neural network of controlled object (fuel valve actuator). a) Training results; b) validation results; c) loss function.

in Fig. 2a. When the control started, the pressure oscillation amplitude gradually attenuated until the oscillation disappeared, and no overshoot occurred during the whole process. The controller output changed abruptly, and it decreased with the decrease of the pressure oscillation amplitude. The weights of the hidden and output layers of the neural network of controller changed gradually in each time step, and reached the final optimal value when oscillation disappeared.

By comparing Figs. 7 and 8, the controller output in the saturation stage was significantly higher than that in the transition stage at the beginning of control, and the step values of the controller output were 0.1 and 0.03, respectively. The final weights of the hidden and output layers of the neural network of controller were slightly lower than those of the transition stage, which were 0.697 and 0.684 compared with 0.699 and 0.697. This indicated that the weights of the neural network of controller updated faster in a single time step when the system oscillation was in the saturation stage. The time intervals from the start of control to the cancellation of oscillation were similar, 0.32 and 0.29 s, respectively.

The training and validation sets for the neural network of controlled object using loudspeaker are shown in Fig. 9. Due to the obvious differences in the governing equations when the fuel valve or loudspeaker is used as actuator, the oscillating pressures caused by the same controller output are significantly different. Compared to Fig. 5, the pressure amplitude was magnified at first, then decreased under the effects of the flat-band output signal taken from pseudo-random number series, and the oscillation amplitude eventually

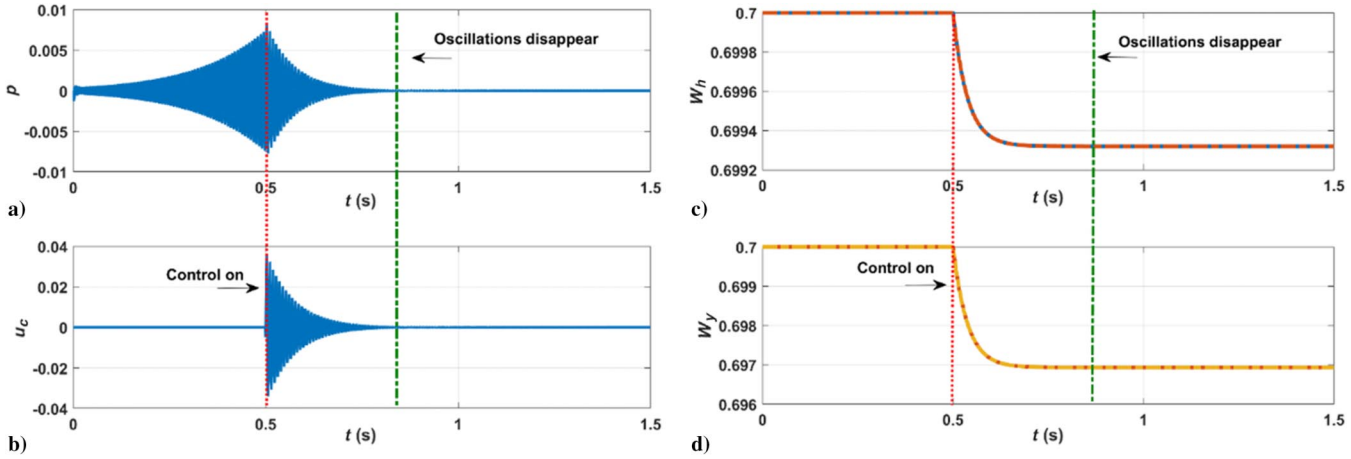

Fig. 7 Active control results (fuel valve actuator/transition stage). a) Normalized pressure; b) controller output; c) hidden layer weights in the neural network of controller; d) output layer weights in the neural network of controller.

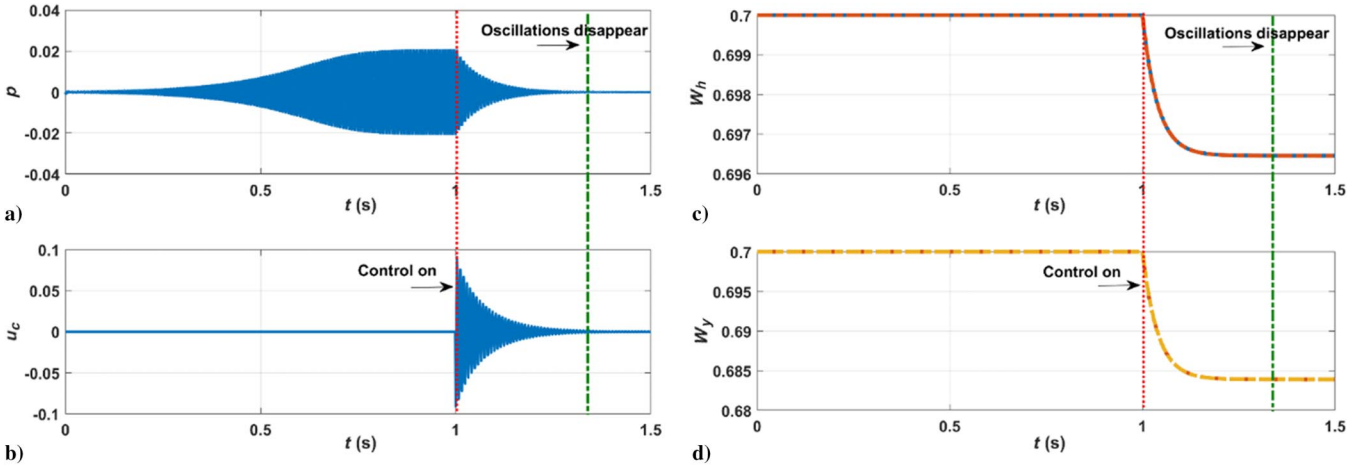

Fig. 8 Active control results (fuel valve actuator/saturation stage). a) Normalized pressure; b) controller output; c) hidden layer weights in the neural network of controller; d) output layer weights in the neural network of controller.

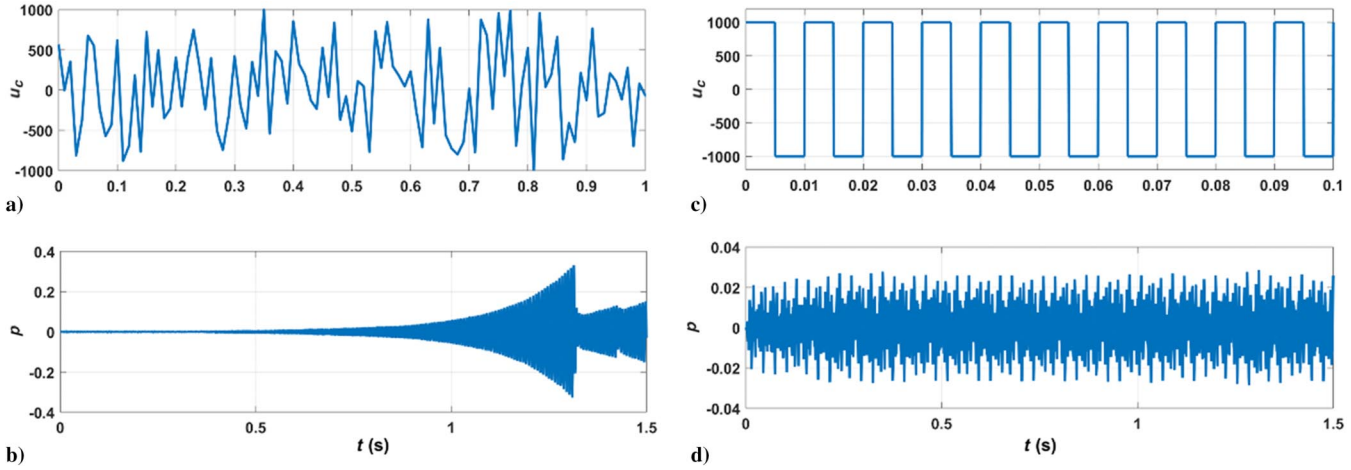

Fig. 9 Training and validation sets of the neural network of controlled object (loudspeaker actuator). a) Controller output for training; b) normalized pressure for training; c) controller output for validation; d) normalized pressure for validation.

maintained within ±0.15. Under the effects of the step output signal, the pressure did not oscillate dramatically in the initial stage, but presented periodic oscillation with amplitude of ±0.03.

Figure 10 shows the training results of the neural network of controlled object. The predicted data from the neural network were highly consistent with the data of the training and validation sets. When the number of training cycles reached 53, the system loss function had the lowest value, indicating that the system training process was over.

Figures 11 and 12 show the active control results of the multiple neural network controller using loudspeaker. In the transition stage, the pressure amplitude first went through a small short-term oscillation when the control started, and then gradually attenuated. The oscillation disappeared at 0.59 s without overshoot in the whole

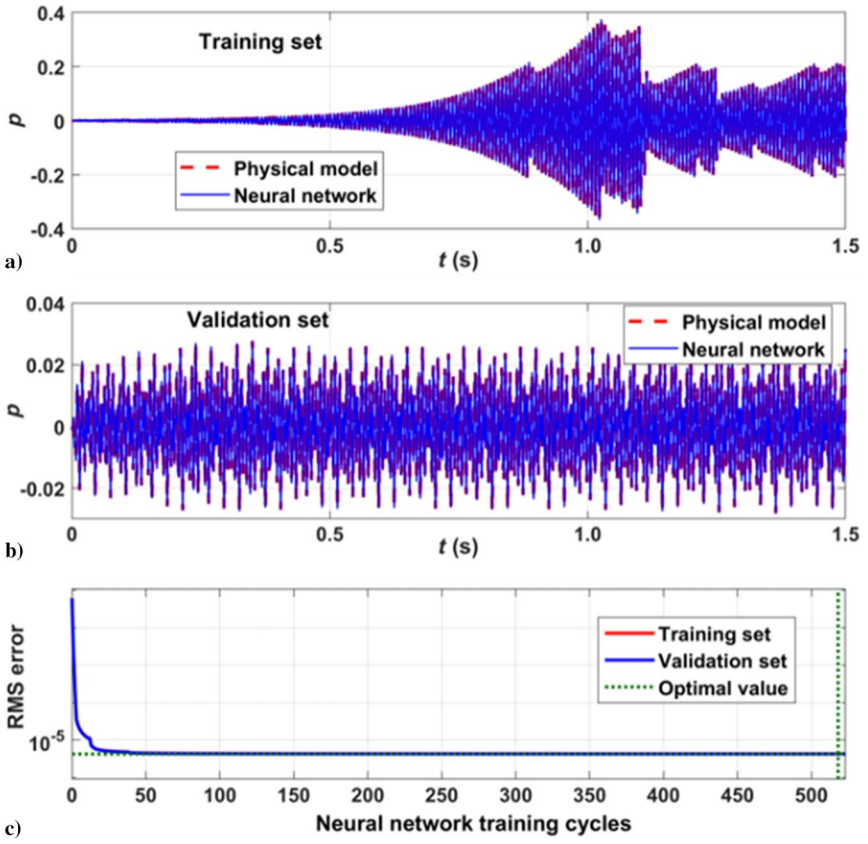

Fig. 10 Training results of the neural network of controlled object (loudspeaker actuator). a) Training results; b) validation results; c) loss function.

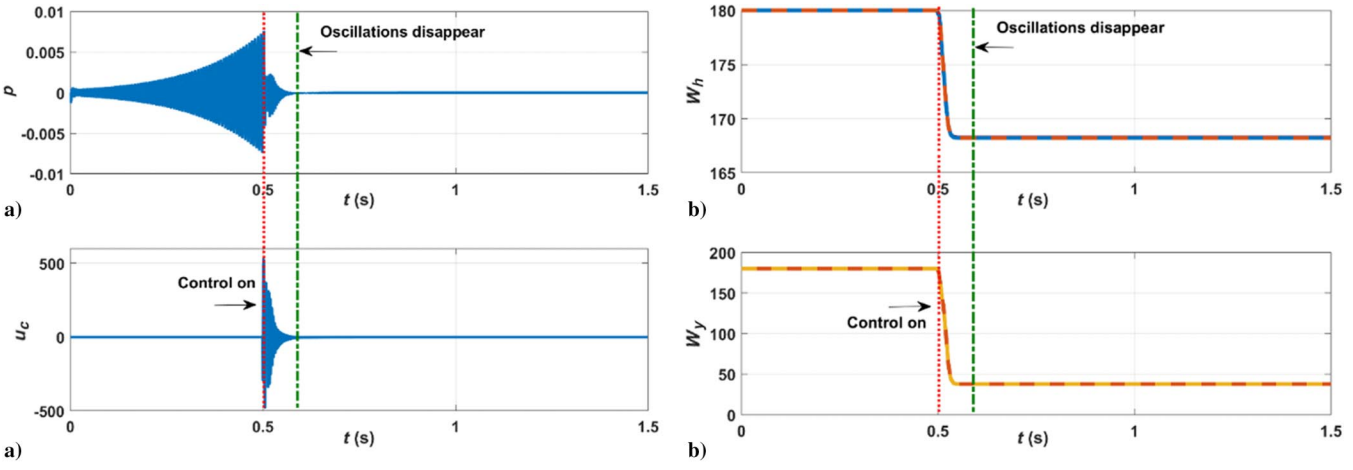

Fig. 11 Active control results (loudspeaker actuator/transition stage). a) Normalized pressure; b) controller output; c) hidden layer weights in the neural network of controller; d) output layer weights in the neural network of controller.

process. The controller output changed abruptly when the control started, and decreased with the decrease of the pressure oscillation amplitude. The weights of the hidden and output layers of the neural network of controller changed gradually in each time step, and reached the final optimal value when the oscillation disappeared. In the saturation stage, the pressure amplitude exceeded the saturation amplitude by 5% when the control started, and then gradually attenuated until the oscillation disappeared at 1.27 s. The characteristics of the weights evolution were similar to those in the transition stage.

By comparing Figs. 11 and 12 with Figs. 7 and 8, it can be found that loudspeaker can suppress the pressure oscillation more quickly than fuel valve in the transition stage. The time intervals from the start of control to the cancellation of oscillation were 0.09 and 0.32 s, respectively. In the saturation stage, the time of eliminating pressure oscillation by loudspeaker and fuel valve was similar, 0.27 and 0.29 s. The pressure amplitude using loudspeaker exceeded the saturation amplitude by 5% in the attenuation process, and the pressure amplitude using fuel valve attenuated smoothly. This was mainly determined by the different effects of the two actuators on the pressure governing equation. The pressure generated by the loudspeaker directly acted on the pressure governing equation [the fourth term of Eq. (15)], whereas the equivalence ratio fluctuations generated by the fuel valve affected the pressure through the flame function [the last term of Eq. (10)], which made the effects of fuel valve on the pressure oscillation more moderate.

B. Effects of Parameter Migration on the Performance

Due to the complexity of practical controlled object, the exact mathematical model of the controlled object may be difficult to obtain. To address this challenge, one can take a simplified model

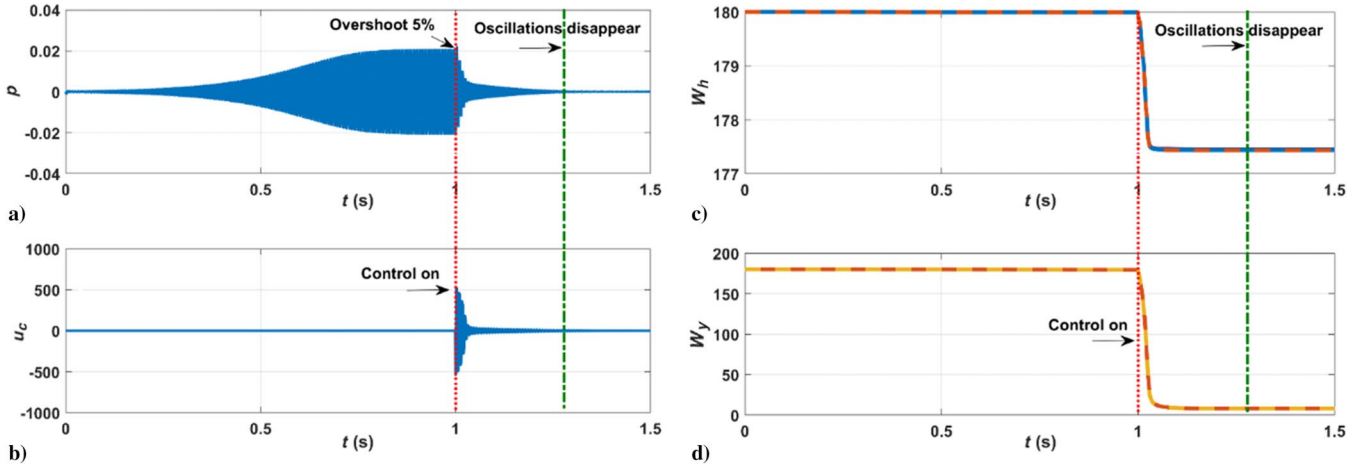

Fig. 12 Active control results (loudspeaker actuator/saturation stage). a) Normalized pressure; b) controller output; c) hidden layer weights in the neural network of controller; d) output layer weights in the neural network of controller.

of the controlled object for the prototype controller and then actively control the practical controlled object through parameter migration. In this study, pretending that the analytical acoustic network model [Eq. (9)] is not available, the following nonlinear 0D state space model [53,54] was employed as a surrogate model of the Rijke tube model system for the prototype controller:

$$\dot{r}_1 = \alpha_1 r_1 - \beta r_1 r_2 \cos(\delta) + u_c \tag{24}$$

$$\dot{r}_2 = \alpha_2 r_2 + \beta r_1^2 \cos(\delta) \tag{25}$$

$$\dot{\delta} = \theta - \beta(r_1^2/r_2 - 2r_2)\sin(\delta) \tag{26}$$

$$p(t) = r_1(t)\sin(t + 0.5\delta(t)) + r_2(t)\sin(2t + \delta(t)) \tag{27}$$

$$\alpha_1 = 0.00647 \tag{28}$$

$$\alpha_2 = -0.021651 \tag{29}$$

$$\beta = 0.221154 \tag{30}$$

$$\theta = -0.035796 \tag{31}$$

where r_1, r_2, and δ are the system state variables, p is the normalized pressure, and u_c is the controller output. The terms of $r_1 r_2$, r_1^2, and r_1^2/r_2 and the trigonometric functions reflect the nonlinearity of this model. This 0D state space model was developed by Kim [52] to study oscillating combustion in rocket motors by linearizing the partial differential conservation equations of mass, momentum, and energy, approximating the extract nonlinear wave equations, applying Green's theorem to reduce the nonlinear wave equations to a system of nonlinear second-order ordinary differential equations, and further reducing to the above first-order nonlinear ordinary differential equations with a time averaging method. However, this model can only represent the variation process of the oscillating combustion pressure at the specific location since it ignores viscous forces, heat transfer, and the spatial distribution of acoustic wave.

Figure 13a shows the evolution of the normalized pressure of the 0D state space model without control. The pressure oscillation went through the linear growth stage, transition stage, and saturation stage, and the final pressure oscillation amplitude remained constant as ± 0.3. By comparing Figs. 2 and 13a, the 0D state space model with the effects of nonlinear factors can reproduce the characteristics of Rijke tube acoustic network model at the measurement position. In contrast, the oscillation pressure amplitude in the 0D linear growth model, which ignores the influence of nonlinear factors on oscillating combustion, increases linearly with time, as shown in Fig. 13b. This model does not consider the effects of nonlinear process, and the results are quite different from the Rijke tube acoustic network model.

In the following, the initial weights of the neural network of Rijke tube controlled object and the neural network of controller is obtained from the optimal training results of the 0D state space model. The effects of parameter migration on the performance of multiple neural

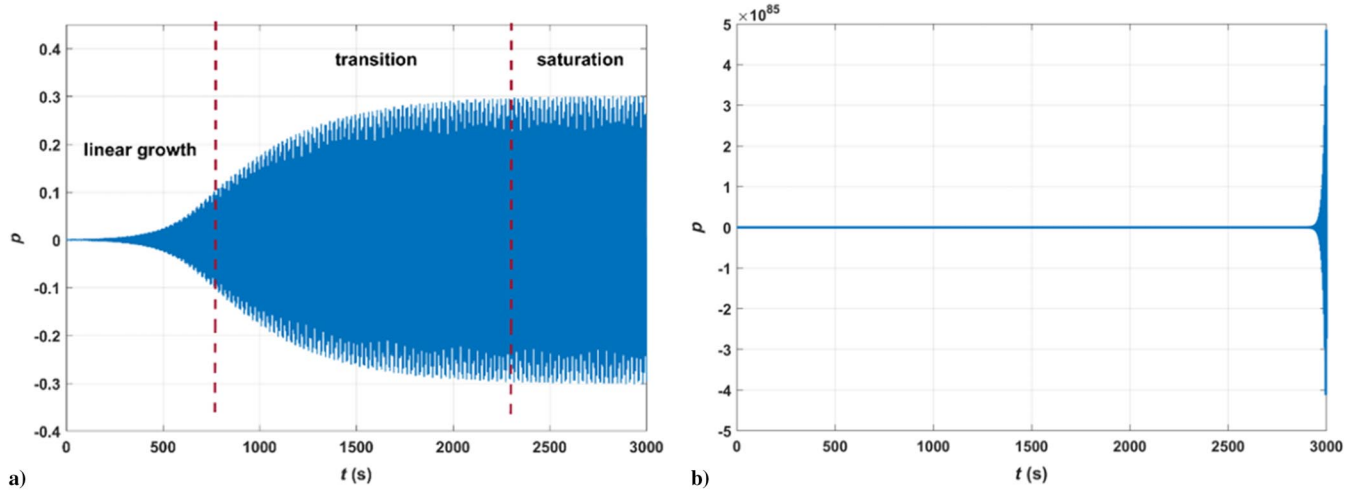

Fig. 13 Pressure evolution of a) 0D state space model and b) 0D linear growth model.

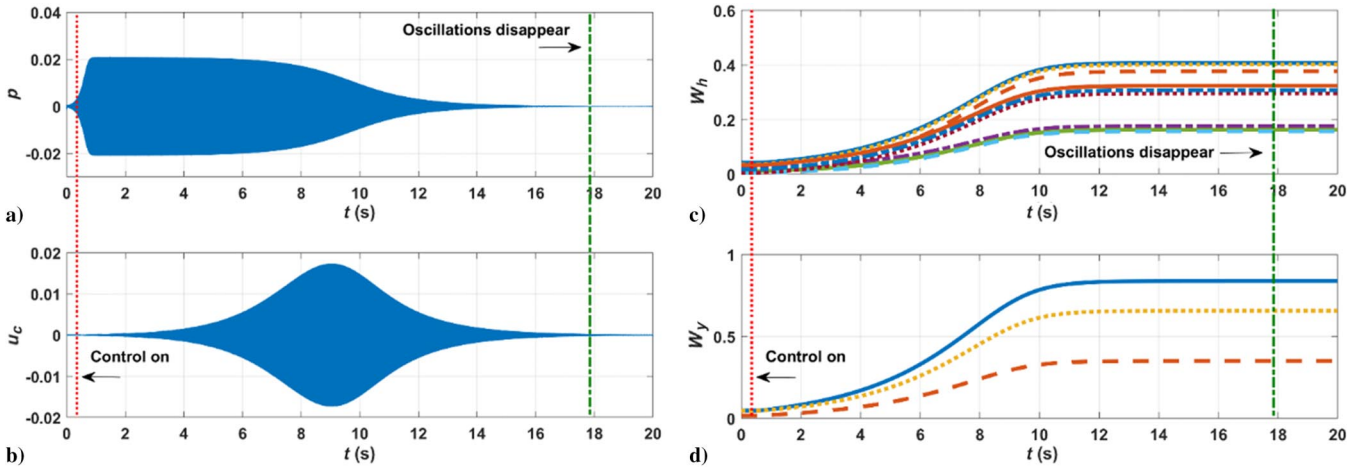

Fig. 14 Effect of parameter migration of 0D state space model on the performance (fuel valve actuators/transition stage). a) Normalized pressure; b) controller output; c) hidden layer weights in the neural network of controller; d) output layer weights in the neural network of controller.

network controller were emphatically investigated. Figure 14 shows the active control results of the Rijke tube combined with 0D state space model. The starting time of control was 0.5 s. Under the effects of the parameter migration, the attenuation process of the system pressure oscillation was obviously prolonged. Although the starting time of the control was in the transition stage, the system oscillation could not be attenuated within this stage, and the oscillation disappeared in the saturation stage at 17.8 s. The controller output increased at first and then decreased. The weights of the hidden and output layers of the neural network of controller changed gradually in each time step without mutation, and reached the final optimal value when the pressure oscillation disappeared. This indicated that

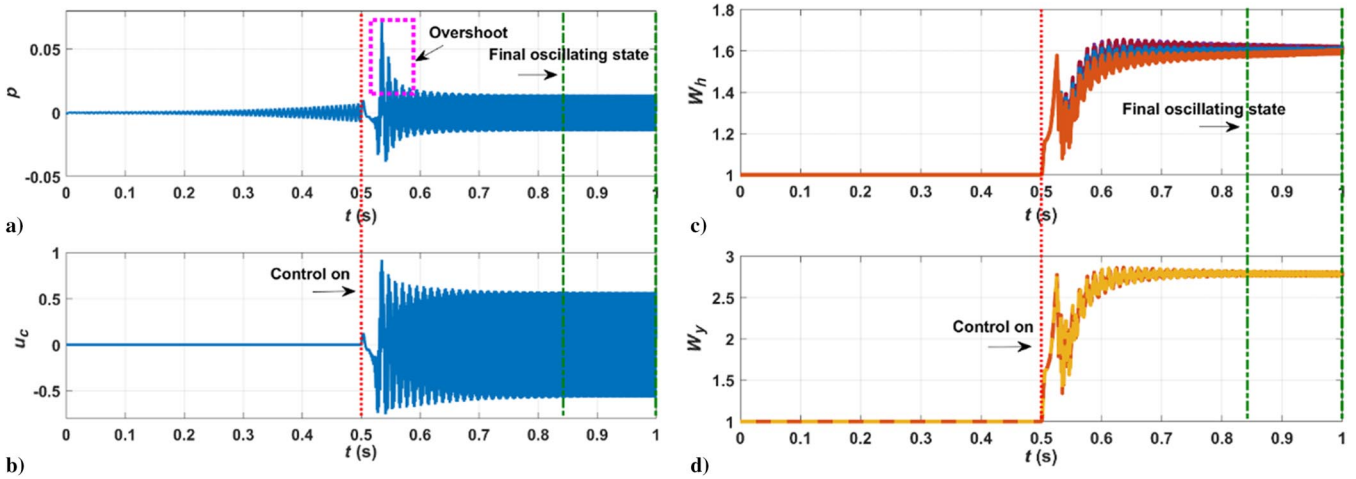

Fig. 15 Effect of parameter migration of 0D linear growth model on the performance (fuel valve actuators/transition stage). a) Normalized pressure; b) controller output; c) hidden layer weights in the neural network of controller; d) output layer weights in the neural network of controller.

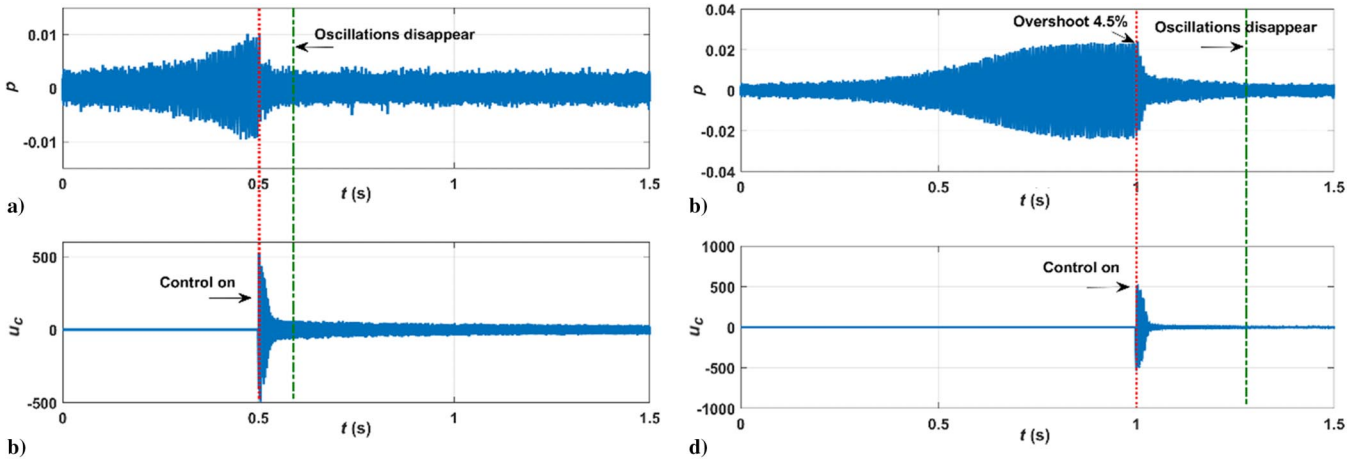

Fig. 16 Effects of noise on the performance (loudspeaker actuators). a) Normalized pressure in transition stage; b) controller output in transition stage; c) normalized pressure in saturation stage; d) controller output in saturation stage.

the parameter migration from the 0D state space model to the Rijke tube acoustic network could effectively realize the controller design and suppress the system oscillation.

To verify the importance of similar characteristics between the 0D model and the Rijke tube model system, the 0D linear growth model that had significantly different characteristics from the Rijke tube as shown in Fig. 13b was adopted to carry out the parameter migration and active control. The results are shown in Fig. 15. It can be seen that the multiple neural network controller could not effectively suppress and eliminate the pressure oscillation due to the inconsistency between the 0D linear growth model and the Rijke tube. The system pressure had an obvious overshoot process, and finally entered a new oscillation state. The evolutions of the controller output and the weights of hidden/output layers of the controller neural network had great mutation and oscillation, which indicated that the premise of active control through parameter migration method was to ensure that the system characteristics of the 0D simplified model and the Rijke tube were similar.

C. Effects of Noise on the Performance

Considering the effects of sensor measurement noise, actuator output noise, and system background noise during the active control

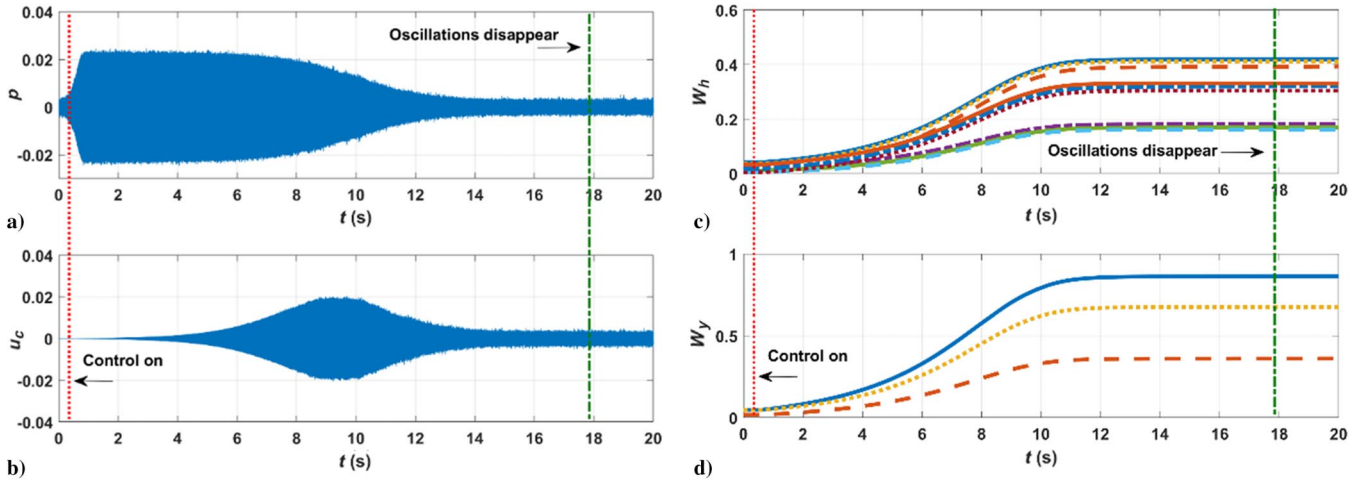

Fig. 17 Effects of noise on the performance with parameter migration of 0D state space model (fuel valve actuators/transition stage). a) Normalized pressure; b) controller output; c) hidden layer weights in the neural network of controller; d) output layer weights in the neural network of controller.

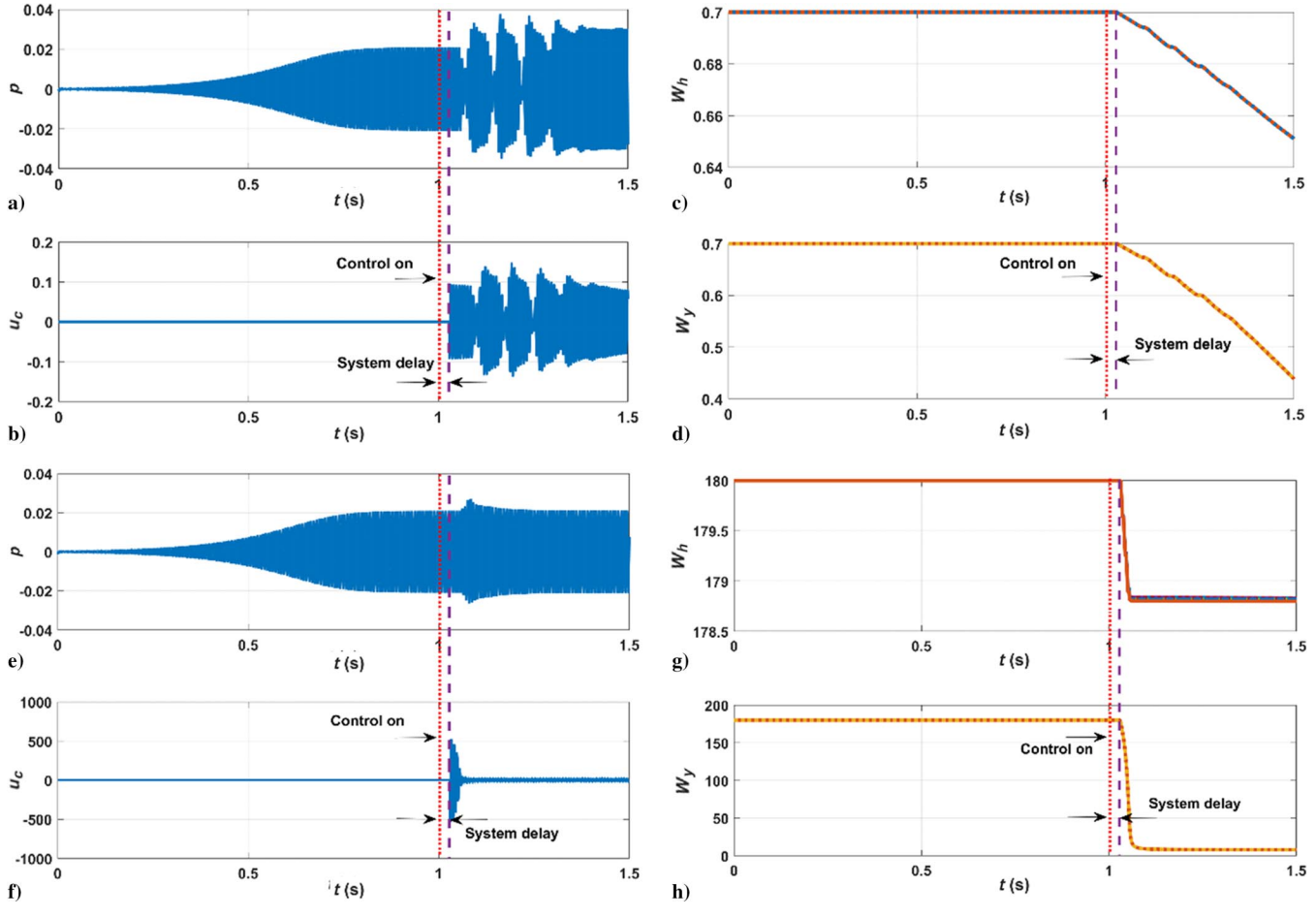

Fig. 18 Effects of delay on active control performance of multiple neural network controller. a–d) Fuel valve as actuator; e–h) loudspeaker as actuator.

process, we show in Fig. 16 the controller performance under the effects of 10% white Gaussian noise using loudspeaker in the Rijke tube acoustic network. The results showed that the multiple neural network controller could effectively suppress and eliminate the system pressure oscillation in the presence of noise, and finally the pressure oscillation amplitude and the controller output were maintained at the noise level, which indicated that this controller was insensitive to noise. Compared with Figs. 12a and 16c, the overshoot of system pressure was reduced from 5% without noise to 4.5% with noise.

Figure 17 shows the effects of noise on the performance using parameter migration method. The results showed that the pressure oscillation and the controller output under the effects of noise had small random fluctuations on the basis of the overall variation trend. When the oscillation disappeared, the controller output still had small fluctuations, but the weights of the hidden and output layers of the neural network of controller always kept smooth and updated, which indicated that the active control performance was not affected by noise when parameter migration method was applied, and it could still effectively suppress and eliminate the pressure oscillation of the Rijke tube system.

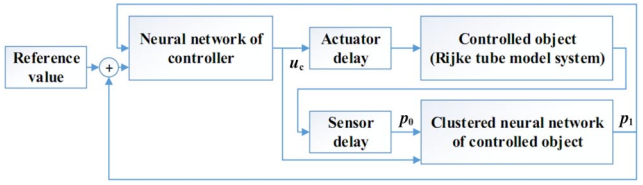

Fig. 19 Structure of the multiple neural network controller considering delay correction.

D. Delay Correction of Multiple Neural Network Controller

Considering the delay effect of sensors and actuators during the active control process, we show in Fig. 18 the performance of multiple neural network controller considering delay effects. The total delay of the sensor and actuator was taken to be 30 ms, and the control starting time was at 1.0 s, corresponding to the saturation stage in Fig. 2. Using fuel valve as actuator, the pressure oscillation appeared periodic overshoot, and finally maintained a new oscillation with greater amplitude. The weights of the hidden and output layers of the neural network of controller deviated linearly from the initial value. Using loudspeaker as actuator, the original saturation amplitude was maintained after a short-term overshoot, and the weights of the hidden and output layers of the neural network of controller tended to a new stable value after rapid adjustment. This indicated that the multiple neural network controller without considering the delay effects could not suppress the pressure oscillation when delay existed in the system. Therefore, the delay correction should be fully considered during the design of controller structure.

The new controller structure considering delay correction in this study is shown in Fig. 19. Sensor delay module and actuator delay module were added, respectively, according to the delay of sensor and actuator. Clustered prediction method [16] was adopted to construct the neural network of controlled object to ensure the accuracy of long-term forecast. The neural network of controlled object based on the clustered prediction method adopted three historical data of system pressure combined with the controller output at the current time step to make clustered prediction for the system pressure data of the next three time steps. In each cycle of the control process, the clustered prediction neural network was iterated with corresponding epochs according to the relationship between the total delay time and the sampling interval. Therefore, the delay was compensated by the iteration of clustered prediction, and the predicted pressure could

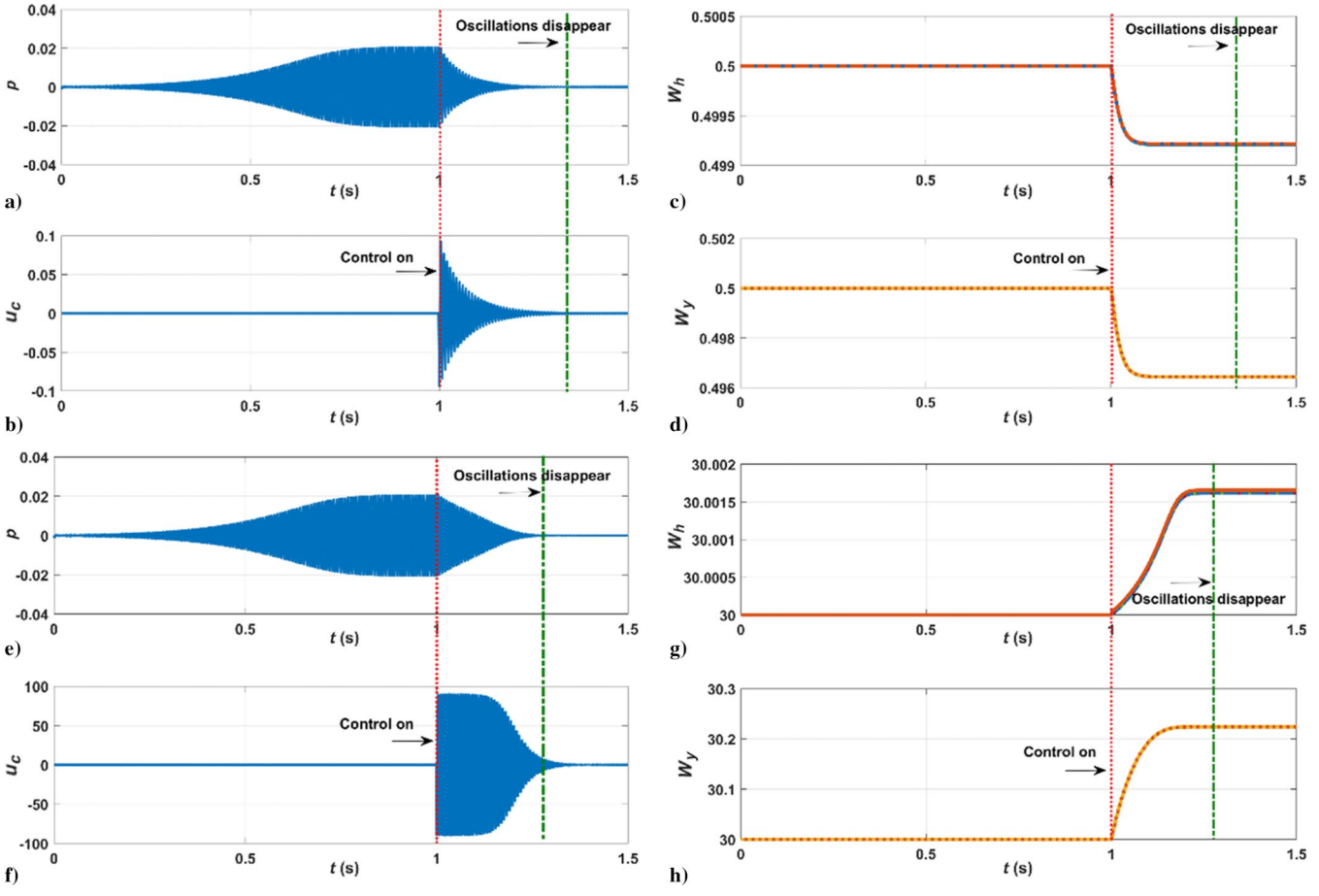

Fig. 20 Controller performance considering delay correction. a–d) Fuel valve as actuator; e–h) loudspeaker as actuator.

offset the effects of sensor and actuator delay. When considering system delay as shown in Fig. 19, the input of the controller neural network is the long-term predicted value p_1, since the existence of system delay requires the controller model to predict and output the control quantity in advance to offset the impact of the delay. This long-term prediction value p_1 is a future prediction of the actual value p_0.

Figure 20 shows the controller performance considering delay correction using fuel valve and loudspeaker as actuator in the Rijke tube acoustic network. Using fuel valve as actuator, the system pressure oscillation was rapidly suppressed after the control started, and finally eliminated. The controller output suddenly changed at the beginning, and then gradually decreased. The weights of the hidden and output layers of the neural network of controller changed gradually in each time step, and reached the optimal value when the pressure oscillation disappeared. Using loudspeaker as actuator, the damping process of the system pressure oscillation was similar to that of using fuel valve. After a short saturation period, the controller output gradually decreased, which indicated that the multiple neural network controller considering delay correction could effectively suppress the system pressure oscillation.

IV. Conclusions

In this study, a multiple neural network controller was proposed to suppress the pressure oscillation of the Rijke tube acoustic network together with the nonlinear flame function. The flame model was based on the classical $n-\tau$ model filtered by a first-order low-pass filter. The nonlinear flame function was achieved by using a gain function saturated with velocity perturbation. Two independent actuators of fuel valve and loudspeaker were adopted. This multiple neural network controller consisted of three modules including two separate neural networks, the neural network of controlled object that is pretrained before control and the neural network of controller that is trained in real time during the control process.

The system pressure oscillation without control can be divided into three stages: linear growth stage, transition stage, and saturation stage. Using the flat-band output signal taken from pseudorandom number series and the step output signal as the training and validation sets, the neural network of controlled object can well fit the variation trend of pressure oscillation, and maintain high precision with both fuel valve and loudspeaker. The weights of the hidden and output layers of the neural network of controller change gradually in each time step when the control starts, and reach the optimal value when oscillation disappears. Thus, the multiple neural network controller could suppress the pressure oscillation amplitude.

When the exact mathematical model of the controlled object is difficult to obtain, the parameter migration from the 0D state space model with similar oscillating characteristics to the Rijke tube acoustic network can effectively achieve the prototype controller design and suppress the system oscillation. But the damping time of the system oscillation is in general longer than that of the controller based on the Rijke tube acoustic network directly. Results further show that the multiple neural network controller is insensitive to noise, and delay correction is achieved by adding sensor and actuator delay modules combined with the clustered prediction method to offset the effects of system delay and suppress the pressure oscillation.

Acknowledgment

This work was supported by National Natural Science Foundation of China (No. 52025062).

References

[1] Nguyen, T. M., and Sirignano, W. A., "Spontaneous and Triggered Longitudinal Combustion Instability in a Single-Injector Liquid-Rocket Combustor," *AIAA Journal*, Vol. 57, No. 12, 2019, pp. 5351–5364. https://doi.org/10.2514/1.J057743

[2] Pavel, P. P., Athanasios, S., and William, A. S., "Low-Probability Events Leading to Rocket Engine Combustion Instability," *AIAA Journal*, Vol. 55, No. 3, 2017, pp. 919–929.

[3] Kazuki, S., Tomokazu, F., Shinji, N., Mitsuhiro, T., Ryuichiro, K., Kyohei, S., Takahiro, I., and Tetsuo, H., "Longitudinal Combustion Instability of a Pintle Injector for a Liquid Rocket Engine Combustor," *Combustion and Flame*, Vol. 194, Aug. 2018, pp. 115–127.

[4] Shinji, N., Hajime, Y., and Mitsuhiro, T., "Experimental Investigation of Ethylene/Air Combustion Instability in a Model Scramjet Combustor Using Image-Based Methods," *Proceedings of the Combustion Institute*, Vol. 38, No. 3, 2021, pp. 3869–3880.

[5] Xiong, J., Hugh, M., Jeremy, K., Feng, L., and William, A. S., "Nonlinear Combustion Instability in a Multi-Injector Rocket Engine," *AIAA Journal*, Vol. 58, No. 1, 2019, pp. 219–235.

[6] Akshay, S., Induja, P., Vishnu, R. U., and Sujith, R. I., "Predicting the Amplitude of Limit-Cycle Oscillations in Thermoacoustic Systems with Vortex Shedding," *AIAA Journal*, Vol. 56, No. 9, 2018, pp. 3507–3514.

[7] Vahid, S., Christian, B., Bertram, J., and Andreas, M. K., "Design and Testing of a High Frequency Thermoacoustic Combustion Experiment," *AIAA Journal*, Vol. 59, No. 8, 2021, pp. 1–17.

[8] Andrea, G., Nicholas, A. W., Epaminondas, M., and Dowling, A. P., "Experimental and Numerical Investigation into the Propagation of Entropy Waves," *AIAA Journal*, Vol. 55, No. 2, 2016, pp. 446–458.

[9] Lee, C. Y., Li, L. K. B., Matthew, P. J., and Robert, S. C., "Nonlinear Hydrodynamic and Thermoacoustic Oscillations of a Bluff-Body Stabilised Turbulent Premixed Flame," *Combustion Theory and Modelling*, Vol. 20, No. 1, 2016, pp. 131–153. https://doi.org/10.1080/13647830.2015.1118555

[10] Shinji, N., Koichi, O., Toshiki, O., Yutaka, I., Che, Z., Mitsuhiro, T., and Hideyuki, T., "Instability and Mode Transition Analysis of a Hydrogen-Rich Combustion in a Model Afterburner," *Proceedings of the Combustion Institute*, Vol. 38, No. 4, 2021, pp. 5933–5942.

[11] Malte, M., Wolfgang, P., Renaud, G., Marco, G., Clément, M., and Thierry, S., "Measurement and Simulation of Combustion Noise and Dynamics of a Confined Swirl Flame," *AIAA Journal*, Vol. 56, No. 5, 2018, pp. 1930–1942.

[12] Karlis, E., Hardalupas, Y., and Taylor, A. M. K. P., "Effects of Inert Fuel Diluents on Thermoacoustic Instabilities in Gas Turbine Combustion," *AIAA Journal*, Vol. 58, No. 6, 2020, pp. 2643–2657. https://doi.org/10.2514/1.J058312

[13] Langella, I., Chen, Z. X., Swaminathan, N., and Sadasivuni, S. K., "Large-Eddy Simulation of Reacting Flows in Industrial Gas Turbine Combustor," *Journal of Propulsion and Power*, Vol. 34, No. 5, 2018, pp. 1269–1284. https://doi.org/10.2514/1.B36842

[14] Moon, K., Choi, Y., and Kim, K. T., "Experimental Investigation of Lean-premixed Hydrogen Combustion Instabilities in a Can-Annular Combustion System," *Combustion and Flame*, Vol. 235, Jan. 2022, pp. 111694–111705.

[15] Zhang, L., Xie, W., and Ren, Z., "Combustion Stability Analysis for Non-Standard Low-Calorific Gases: Blast Furnace Gas and Coke Oven Gas," *Fuel*, Vol. 278, No. 1, 2020, pp. 118216–118226.

[16] Zhang, L., Xue, Y., Xie, Q., and Ren, Z., "Analysis and Neural Network Prediction of Combustion Stability for Industrial Gases," *Fuel*, Vol. 287, No. 5, 2021, pp. 119507–119518.

[17] Zhang, L., Wang, N., Wei, J., and Ren, Z., "Exploring Active Subspace for Neural Network Prediction of Oscillating Combustion," *Combustion Theory and Modelling*, Vol. 25, No. 3, 2021, pp. 570–587. https://doi.org/10.1080/13647830.2021.1915500

[18] Li, B., Shi, B., Zhao, X., Ma, K., Xie, D., Zhao, D., and Li, J., "Oxy-fuel Combustion of Methane in a Swirl Tubular Flame Burner Under Various Oxygen Contents: Operation Limits and Combustion Instability," *Experimental Thermal and Fluid Science*, Vol. 90, Jan. 2018, pp. 115–124. https://doi.org/10.1016/j.expthermflusci.2017.09.001

[19] Zhou, H., and Sheng, M., "Numerical Prediction of Swirl Burner Geometry Effects on NOx Emission and Combustion Instability in Heavy Oil-fired Boiler," *Applied Thermal Engineering*, Vol. 159, Aug. 2019, pp. 113,843–113,853.

[20] Lieuwen, T., and Yang, V., *Combustion Instabilities in Gas Turbines, Operational Experience, Fundamental Mechanisms, and Modeling*, Progress in Astronautics and Aeronautics, AIAA, Washington, D.C., 2005, Chap. 12.

[21] Lieuwen, T. C., *Unsteady Combustor Physics*, 1st ed., Cambridge Univ. Press, Cambridge, England, U.K., 2012, Chap. 6.

[22] Poinsot, T., and Veynante, D., *Theoretical and Numerical Combustion*, 2nd ed., R. T. Edwards, Ipswich, Austrilia, 2005, Chap. 8.

[23] Kim, K. T., "Nonlinear Interactions Between the Fundamental and Higher Harmonics of Self-Excited Combustion Instabilities," *Combustion Science and Technology*, Vol. 189, No. 7, 2017, pp. 1091–1106. https://doi.org/10.1080/00102202.2016.1275591

[24] Sharifi, V., Kempf, A. M., and Beck, C., "Large-Eddy Simulation of Acoustic Flame Response to High-Frequency Transverse Excitations,"

AIAA Journal, Vol. 57, No. 1, 2019, pp. 327–340.
https://doi.org/10.2514/1.J056818

[25] Bernardini, M., Cimini, M., Stella, F., Cavallini, E., Mascio, A. D., Neri, A., and Martelli, E., "Large-Eddy Simulation of Vortex Shedding and Pressure Oscillations in Solid Rocket Motors," *AIAA Journal*, Vol. 58, No. 6, 2020, pp. 5191–5201.

[26] Zhao, M., Ye, T., and Li, Q., "Large-Eddy Simulations of Transverse Jet Mixing and Flame Stability in Supersonic Crossflow," *AIAA Journal*, Vol. 59, No. 6, 2021, pp. 2126–2142.

[27] Huang, Z., Guo, T., Han, X., and Mao, J., "Very Large Eddy Simulation of Lean Premixed Flames to Imposed Inlet Velocity Oscillations," *Combustion Science and Technology*, Vol. 24, May 2021, pp. 1–24.

[28] Xu, J., Huang, C., and Karthik, D., "Reduced-Order Modeling Framework for Combustor Instabilities Using Truncated Domain Training," *AIAA Journal*, Vol. 58, No. 2, 2019, pp. 618–632.

[29] Gonzalez-Flesca, M., Scouflaire, P., Schmitt, T., Ducruix, S., Candel, S., and Méry, Y., "Reduced Order Modeling Approach to Combustion Instabilities of Liquid Rocket Engines," *AIAA Journal*, Vol. 56, No. 12, 2018, pp. 4845–4857.
https://doi.org/10.2514/1.J057098

[30] Mahmoudi, Y., Dowling, A. P., and Stow, S. R., "Acoustic and Entropy Waves in Nozzles in Combustion Noise Framework," *AIAA Journal*, Vol. 55, No. 7, 2017, pp. 2369–2381.
https://doi.org/10.2514/1.J055597

[31] William, A. S., and Pavel, P. P., "Two-Dimensional Model for Liquid-Rocket Transverse Combustion Instability," *AIAA Journal*, Vol. 51, No. 12, 2013, pp. 2919–2934.

[32] Akshay, S., Vineeth, N., and Sujith, R. I., "A Reduced-Order Deterministic Model Describing an Intermittency Route to Combustion Instability," *Combustion Theory and Modelling*, Vol. 20, No. 3, 2016, pp. 441–456.

[33] Chae, H., and Lee, C., "Controlling Low-Frequency Instability with Fuel Inserts in Hybrid Rocket Combustion," *Journal of Propulsion and Power*, Vol. 37, No. 1, 2021, pp. 13–19.
https://doi.org/10.2514/1.B37972

[34] John, W. B., Robert, A. F., Jacob, T. C., and David, M. L., "Combustion Instability Control Through Acoustic Modulation at the Inlet Boundary: Experiments," *Journal of Propulsion and Power*, Vol. 31, No. 6, 2015, pp. 1672–1688.

[35] John, W. B., Sarma, L. R., Jacob, T. C., and Robert, A. F., "Combustion Instability Control Through Acoustic Modulation at the Inlet Boundary: Analysis," *Journal of Propulsion and Power*, Vol. 31, No. 6, 2015, pp. 1689–1695.

[36] John, C. D., George, K., Joseph, R. S., Clarence, T. C., and Wey, C., "Active Combustion Control for a Low-Emissions Aircraft Engine Combustor Prototype: Experimental Results," *Journal of Propulsion and Power*, Vol. 29, No. 4, 2013, pp. 991–1000.

[37] Morgans, A., and Dowling, A., "Model-Based Control of Combustion Instabilities," *Journal of Sound and Vibration*, Vol. 299, Jan. 2007, pp. 261–282.
https://doi.org/10.1016/j.jsv.2006.07.014

[38] Dowling, A., and Morgans, A., "Feedback Control of Combustion Oscillations," *Annual Review of Fluid Mechanics*, Vol. 37, No. 1, 2005, pp. 151–182.
https://doi.org/10.1146/annurev.fluid.36.050802.122038

[39] Annaswamy, A. M., and Ghoniem, A. F., "Active Control of Combustion Instability: Theory and Practice," *IEEE Control Systems Magazine*, Vol. 22, No. 6, 2003, pp. 37–54.

[40] Zhang, G., Wang, X., Li, L., and Sun, X., "Effects of Perforated Liners on Controlling Combustion Instabilities in Annular Combustors," *AIAA Journal*, Vol. 58, No. 7, 2020, pp. 3100–3114.

[41] Zhao, D., Morgans, A. S., and Dowling, A. P., "Tuned Passive Control of Acoustic Damping of Perforated Liners," *AIAA Journal*, Vol. 49, No. 4, 2011, pp. 725–734.
https://doi.org/10.2514/1.J050613

[42] Linck, M., and Gupta, A. K., "Passive Control of Forced Combustion Instability in a Swirl-Stabilized Spray Combustor," *Journal of Propulsion and Power*, Vol. 23, No. 5, 2007, pp. 1113–1122.
https://doi.org/10.2514/1.15933

[43] Annaswamy, A., Fleifil, M., Rumsey, J., Prasanth, R., Hathout, J. P., and Ghoniem, A. F., "Thermoacoustic Instability: Model-based Optimal Control Designs and Experimental Validation," *IEEE Transactions on Control Systems Technology*, Vol. 8, No. 6, 2000, pp. 905–918.
https://doi.org/10.1109/87.880593

[44] Chu, Y. C., Dowling, A. P., and Glover, K., "Robust Control of Combustion Oscillations," *Proceedings of the 1998 IEEE International Conference on Control Applications*, Trieste, Italy, Sept. 1998.

[45] Hathout, J. P., Fleifil, M., Annaswamy, A. M., and Ghoniem, A. F., "Active Control Using Fuel-Injection of Time-Delay Induced Combustion Instability," *Journal of Propulsion and Power*, Vol. 18, No. 1, 2002, pp. 390–399

[46] Evesque, S., and Dowling, A. P., "LMS Algorithm for Adaptive Control of Combustion Oscillations," *Combustion Science and Technology*, Vol. 164, No. 1, 2001, pp. 65–93.
https://doi.org/10.1080/00102200108952162

[47] Zhang, L., Li, S., Xue, Y., Zhou, H., and Ren, Z., "Neural Network PID Control for Combustion Instability," *Combustion Theory and Modelling*, Vol. 1, No. 16, 2022, pp. 1–16.

[48] Li, S., Zhao, D., Ji, C., and Li, J., "Combustion Instabilities in a Bifurcating Tube: Open- and Closed-Loop Measurements," *AIAA Journal*, Vol. 52, No. 11, 2014, pp. 2513–2523.
https://doi.org/10.2514/1.J052758

[49] Bradley, R. H., and Kunning, G. X., "Electric Field Damping of Rijke Tube Combustion Instabilities," *Journal of Propulsion and Power*, Vol. 34, No. 1, 2017, pp. 85–96.

[50] Dowling, A. P., "The Calculation of Thermoacoustic Oscillations," *Journal of Sound and Vibration*, Vol. 180, No. 4, 1995, pp. 557–581.
https://doi.org/10.1006/jsvi.1995.0100

[51] Crocco, L., "Aspects of Combustion Stability in Liquid Propellant Rocket Motors Part I: Fundamentals. Low Frequency Instability with Monopropellants," *Journal of the American Rocket Society*, Vol. 21, No. 6, 2012, pp. 163–178.
https://doi.org/10.2514/8.4393

[52] Li, J., and Morgans, A. S., "Model Based Control of Nonlinear Combustion Instabilities," *21st International Congress on Sound and Vibration (ICSV21) (No. 25411)*, Beijing, China, July 2014.

[53] Kim, S., and Kim, S., "Nonlinear Combustion Instabilities in Combustion Chambers," Ph.D. Dissertation, Pennsylvania State Univ., State College, PA, 1989.

[54] Blonbou, R., Laverdant, A., Zaleski, S., and Kuentzmann, P., "Active Adaptive Combustion Control Using Neural Networks," *Combustion Science and Technology*, Vol. 156, No. 1, 2000, pp. 25–47.
https://doi.org/10.1080/00102200008947295

Y. Ju
Associate Editor